

STRUCTURE NOTE

Crystal structure of juvenile hormone epoxide hydrolase from the silkworm *Bombyx mori*

Kang Zhou,¹ Ning Jia,¹ Chen Hu,¹ Yong-Liang Jiang,¹ Jie-Pin Yang,¹ Yuxing Chen,¹ Sheng Li,^{2*} Wei-Fang Li,^{1*} and Cong-Zhao Zhou^{1*}

¹Hefei National Laboratory for Physical Sciences at the Microscale, and School of Life Sciences, University of Science and Technology of China, Hefei, Anhui, 230027, People's Republic of China

²Key Laboratory of Developmental and Evolutionary Biology, Institute of Plant Physiology and Ecology, Shanghai Institutes for Biological Sciences, Chinese Academy of Sciences, Shanghai, 200032, People's Republic of China

INTRODUCTION

The juvenile hormone (JH) is a kind of epoxide-containing sesquiterpene ester secreted by a pair of corpora allatum behind the brain of insects.¹ It controls the metamorphosis development of insects together with the ecdysone.^{2,3} Thus the synthesis and degradation of JH are tightly regulated in different development stages.⁴ The degradation of JH is catalyzed by two hydrolases, juvenile hormone epoxide hydrolase (JHEH) and juvenile hormone esterase. JHEH is responsible for opening the epoxide ring of JH to produce JH diol, whereas JHE catalyzes the removal of the methyl ester moiety of JH to form JH acid.^{5,6} JHEH belongs to the microsomal epoxide hydrolase (mEH) (*EC* 3.3.2.9) family, which is one of the most widely distributed families of epoxide hydrolases (EHs). EHs can transform epoxides to compounds with decreased chemical reactivity, increased water solubility, and altered biological activity.^{7,8} In addition to participating in the catabolism of JH in insects, mEHs also play important roles in cytoprotection, steroid metabolism, bile acid transport, and xenobiotic metabolism.⁹

To date, the only structure of the mEH from the fungus *Aspergillus niger* (termed AnEH, PDB 1QO7) revealed a typical α/β -hydrolase core composed of a twisted eight-stranded β -sheet packing on both sides with several α -helices.^{10,11} Structural analyses suggested a bimolecular nucleophilic substitution (S_N2) reaction mechanism involving a standard nucleophile–histidine–acid catalytic triad of Asp–His–Glu/Asp.¹¹ However, the mechanism of substrate recognition and catalysis of mEHs remains

unclear. Here we report the crystal structure of *Bombyx mori* JHEH (BmJHEH) at 2.30 Å resolution. Structural analyses together with molecular simulation reveal insights into the specific binding of JH in the active-site pocket. These findings increase our understanding of the substrate recognition and catalysis of mEHs and might help the design of JH-derived pesticides.

MATERIALS AND METHODS

Construction, expression, and purification of BmJHEH

The *BmJHEH* gene without signal peptide was amplified and cloned into a pET29a-derived expression vector with an N-terminal 6×His-tag. The recombinant plasmid was transformed into *E. coli* BL21 (DE3) strain (Novagen) cultured in 2×YT medium (16 g of Bacto-Tryptone, 10 g of yeast

Grant sponsor: Ministry of Science and Technology of China; grant number: 2012CB114600; Grant sponsor: National Natural Science Foundation of China; grant number: 31272362.

*Correspondence to: Cong-Zhao Zhou; Hefei National Laboratory for Physical Sciences at the Microscale, and School of Life Sciences, University of Science and Technology of China, Hefei, Anhui 230027, People's Republic of China. E-mail: zcz@ustc.edu.cn or Wei-Fang Li; Hefei National Laboratory for Physical Sciences at the Microscale, and School of Life Sciences, University of Science and Technology of China, Hefei, Anhui 230027, People's Republic of China. E-mail: liwf@ustc.edu or Sheng Li; Key Laboratory of Developmental and Evolutionary Biology, Institute of Plant Physiology and Ecology, Shanghai Institutes for Biological Sciences, Chinese Academy of Sciences, Shanghai 200032, People's Republic of China. E-mail: shengli@sippe.ac.cn.

Received 28 June 2014; Revised 28 July 2014; Accepted 6 August 2014
Published online 21 August 2014 in Wiley Online Library (wileyonlinelibrary.com). DOI: 10.1002/prot.24676

Table 1
Data Collection and Refinement Statistics

Data collection	
Space group	<i>C2</i>
Unit cell	161.40, 51.47, 124.45
<i>a</i> , <i>b</i> , <i>c</i> (Å)	90.00, 122.68, 90.00
α , β , γ (°)	
Resolution range (Å)	50.00–2.30 (2.38–2.30) ^a
Wilson B factor (Å ²)	32.19
Unique reflections	38,204 (3,671)
Completeness (%)	99.2 (96.7)
$\langle I/\sigma(I) \rangle$	11.8 (2.9)
R_{merge}^b (%)	10.8 (50.0)
Average redundancy	4.0 (3.5)
Structure refinement	
Resolution range (Å)	50.00–2.30
R-factor ^c /R-free ^d (%)	20.6/25.1
Number of protein atoms	6,655
Number of water atoms	159
RMSD ^e bond lengths (Å)	0.006
RMSD ^e bond angles (°)	1.067
Mean B factors (Å ²)	33.92
Ramachandran plot	
Most favored (%)	96.61
Additional allowed (%)	3.39
Outliers (%)	0
PDB entry	4QLA

^aThe values in parentheses refer to statistics in the highest bin.

^b $R_{\text{merge}} = \sum_{\text{hkl}} \sum_i |I_i(\text{hkl}) - \langle I(\text{hkl}) \rangle| / \sum_{\text{hkl}} \sum_i I_i(\text{hkl})$, where $I_i(\text{hkl})$ is the intensity of an observation and $\langle I(\text{hkl}) \rangle$ is the mean value for its unique reflection; Summations are over all reflections.

^c $R\text{-factor} = \sum_{\text{hkl}} |F_o(\text{h}) - F_c(\text{h})| / \sum_{\text{hkl}} F_o(\text{h})$, where F_o and F_c are the observed and calculated structure-factor amplitudes, respectively.

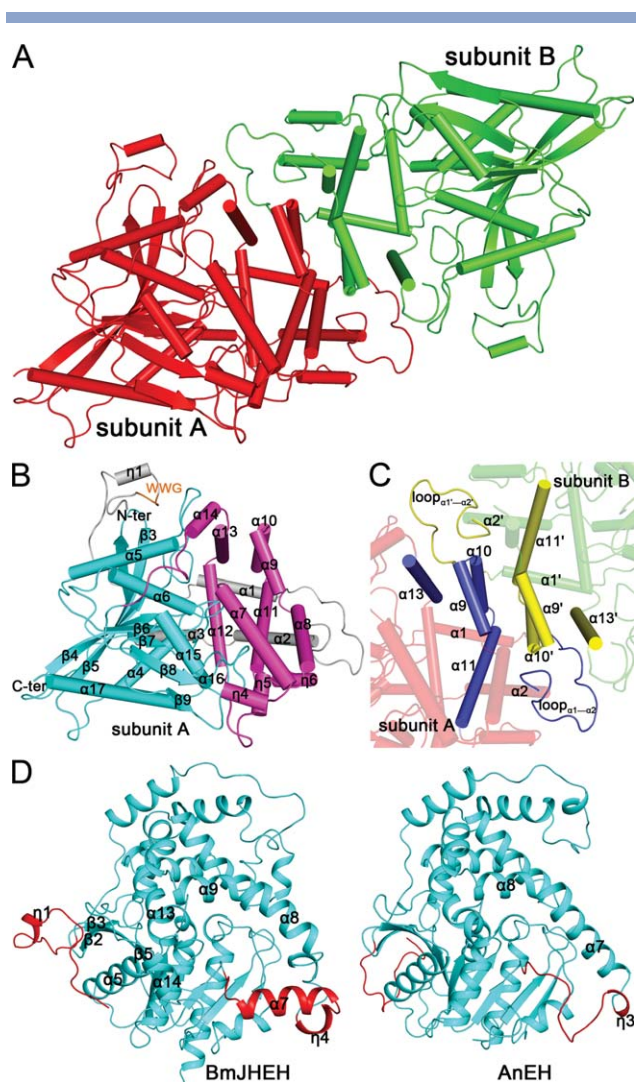
^dR-free was calculated with 5% of the data excluded from the refinement.

^eRoot-mean square-deviation from ideal values.

extract and 5 g of NaCl per liter) containing 30 $\mu\text{g/mL}$ kanamycin. The cells were grown at 37°C to an $\text{OD}_{600\text{nm}}$ of 0.7. Expression of the proteins was induced with 0.2 mM isopropyl- β -D-1-thiogalactoside. Cells were cultured for another 20 h at 16°C and were then collected by centrifugation and resuspended in the lysis buffer (20 mM Tris-HCl, pH 8.0, 100 mM NaCl, 14 mM β -mercaptoethanol). After freezing/thawing in liquid nitrogen, 5 min of sonication and centrifugation at 12,000g for 30 min, the soluble target protein was collected and loaded onto a Ni-NTA column (Amersham Biosciences) equilibrated with the lysis buffer. The target protein was eluted with 300 mM imidazole, and further purified by gel filtration in a Superdex 200 column (GE Healthcare) equilibrated with 20 mM Tris-HCl, pH 8.0, 100 mM NaCl and 14 mM β -mercaptoethanol. Fractions containing the target protein were pooled and concentrated to 14 mg/mL by ultrafiltration (Millipore Amicon) for crystallization. The protein purity was assessed by electrophoresis and the protein sample was stored at -80°C .

Crystallization, data collection, and processing

The purified protein was methylated before crystallization. Crystallization was carried out at 289 K using the

**Figure 1**

Overall structure of BmJHEH. (A) The dimeric structure. The subunits A and B are colored red and green, respectively. (B) Three parts of subunit A are colored gray for the N-terminal region (Leu33–Tyr118), cyan for the α/β domain (Pro119–Leu255 and Gln392–Asn456) and pink for the lid domain (Ser256–Val391), respectively. The “WWG” motif is labeled in orange. The secondary structural elements are labeled sequentially. (C) Residues involved in dimeric interaction are colored blue in subunit A and yellow in subunit B, respectively. The other residues of two subunits were shown with transparency. (D) Structural comparison between BmJHEH and AnEH. The similar parts are colored cyan, whereas the different segments are colored red.

hanging drop vapor-diffusion technique. Drops were prepared by mixing 1 μL protein solution containing 20 mM dithiothreitol with 1 μL mother liquor (0.1 M Tris-HCl, pH 8.0, 19% polyethylene glycol 2000). The crystals appeared in 2 months. A single crystal was transferred to the cryoprotectant of the reservoir solution supplemented with 20% glycerol and flash-cooled with liquid nitrogen. The X-ray diffraction data were collected on a MarResearch 345 image-plate detector using beamline 17U at the Shanghai Synchrotron Radiation Facility

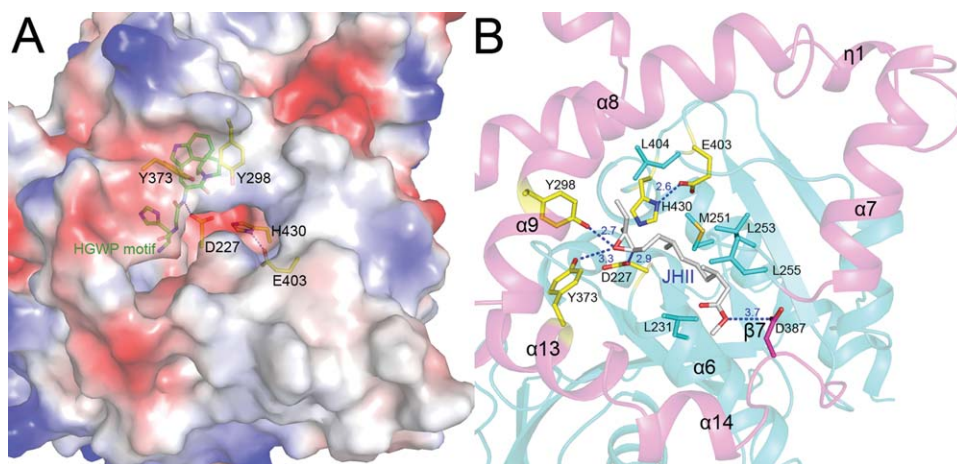


Figure 2

The putative JHII-binding pattern. (A) The surface electrostatic potential of JHII-binding pocket. The catalytic triad (Asp227, His430, and Glu403) and two tyrosine residues (Tyr298 and Tyr373) are shown as yellow sticks. The HGWP motif is shown as green sticks. (B) The simulated model of JHII binding to BmJHEH. JHII is shown in gray sticks. The JHII-binding residues are shown as sticks.

(SSRF). The data were processed with the program HKL2000.¹²

Structure solution and refinement

The crystal structure of BmJHEH was solved by the molecular replacement method with the program MOLREP¹³ using the structure of *A. niger* EH (PDB code 1QO7) as the search model. Crystallographic refinement was performed using the program REFMAC5,¹⁴ as a part of CCP4i¹⁵ program suite. Several rounds of manual rebuilding were carried out using the graphics program COOT.¹⁶ The water molecules were then placed into the electron density map. The structure was finally refined to 2.30 Å with an R_{factor} of 20.6% and R_{free} of 25.1%. The final model was evaluated with the program MOLPROBITY.¹⁷ The statistics and refinement parameters were listed in Table I. All figures of protein structure were prepared with PyMol.¹⁸

Remodeling of the substrate binding site

Docking of JHII (methyl (2E,6E)-10R,11S-(oxiranyl)-3,7,11-trimethyl-2,6-tridecadienoate) to the active site of BmJHEH was performed using the program HADDOCK.¹⁹ The output gave 20 similar structures in one cluster with the lowest HADDOCK score, among which we chose the most reliable model according to the optimal steric distances between JHII and the surrounding residues.

Accession number

The final coordinates and structure factors were deposited in the Protein Data Bank under the accession code of 4QLA.

RESULTS AND DISCUSSION

Overall structure

The structure of BmJHEH at 2.30 Å resolution was determined by molecular replacement method using the AnEH structure (PDB 1QO7) as the search model. Each asymmetric unit contains two subunits, which are almost identical to each other with a root-mean square-deviation (RMSD) of 0.24 Å over 309 C α atoms [Fig. 1(A)]. In the final model, subunit A contains residues Leu33–Asn456, whereas subunit B has two untraced segments Leu253–Ser290 and Asp383–Glu388 because of the poor electron density. Thus we took subunit A as an example for the following structural analyses.

Subunit A consists of three parts: an N-terminal segment (Leu33–Tyr118) followed by a core hydrolase domain (residues Pro119–Leu255 and Gln392–Asn456), which is interrupted by an all- α lid domain (Ser256–Val391) [Fig. 1(B)]. The core domain adopts a typical α/β hydrolase fold, which is composed of a twisted mixed β -sheet ($\beta 2$ – $\beta 9$) packed on both sides with α -helices $\alpha 4$ – $\alpha 6$ and $\alpha 15$ – $\alpha 17$, respectively. The lid domain, which consists of eight α -helices ($\alpha 7$ – $\alpha 14$) and three η -helices ($\eta 4$ – $\eta 6$), interrupts the core domain by inserting between $\beta 7$ and $\beta 8$. The N-terminal segment contains a η -helix ($\eta 1$) and three α -helices ($\alpha 1$ – $\alpha 3$), which form a long curved meander covering a part of the lid and core domains. Notably, the N-terminal segment contains a conserved ‘XWG’ motif (where X is an aromatic residue, corresponding to W³⁸WG⁴⁰), which was proposed to be required for the localization of BmJHEH to the endoplasmic reticulum.²⁰ This motif has been found to function as an anchor for the membrane association and

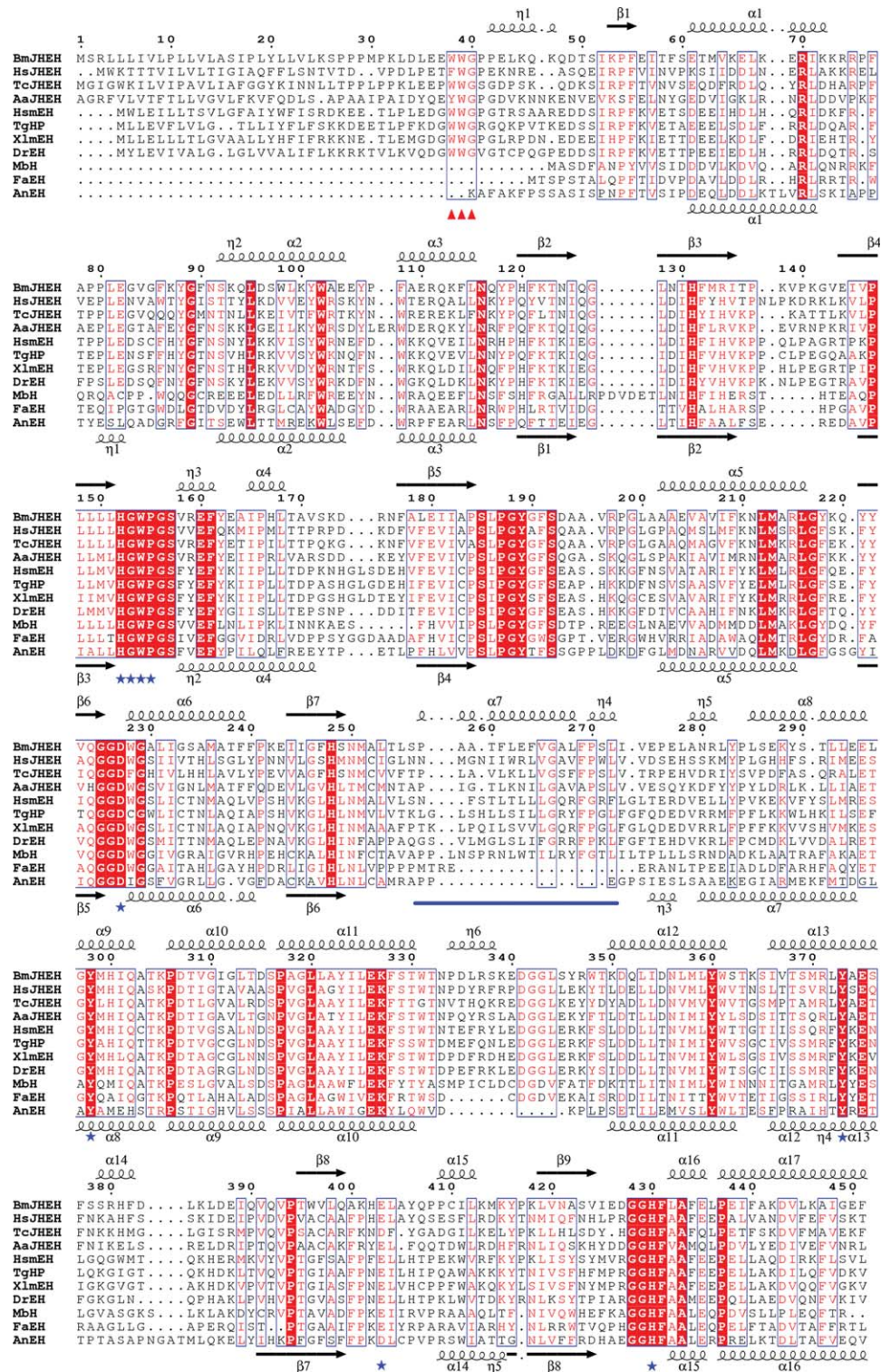


Figure 3

Multiple-sequence alignment of BmJHEH and homologs. The N-terminal membrane anchor motif "XWG" is labeled as red triangles. The catalytic triad (Asp227, His430, and Glu403), HGWP motif and two tyrosine residues (Tyr298 and Tyr373) are labeled as blue stars. The insertion segment α7 and η4 is marked by a blue line. The multisequence alignment was performed using programs ClustalW2 (<http://www.ebi.ac.uk/Tools/msa/clustalw2/>) and ESPript (<http://esprpt.ibcp.fr/ESPrpt/cgibin/ESPrpt.cgi>). All sequences were downloaded from the NCBI database (www.ncbi.nlm.nih.gov). The sequences are (NCBI accession numbers codes are in parentheses) *Bombyx mori* JHEH 1 (NP_001037201.1), *Harpegnathos saltator* JHEH 1 (EFN83232.1), *Tribolium castaneum* JHEH-like protein 3 (NP_001161906.1), *Aedes aegypti* JHEH (AAM88326.1), *Homo sapiens* mEH (AAC41694.1), *Taeniopygia guttata* predicted EH 1 (XP_002194617.1), *Xenopus laevis* EH 1, microsomal (xenobiotic) precursor (NP_001085033.1), *Danio rerio* EH 1 (NP_957362.1), *Monosiga brevicollis* MX1 hypothetical protein (XP_001743954.1), *Frankia alni* ACN14a EH (YP_713944.1), *Aspergillus niger* EH (CAB59812.1).

subcellular localization of mEHs in higher organisms as well.^{21,22}

The two subunits of BmJHEH in an asymmetric unit form a stable dimer with a total buried interface area of 4700 Å². Gel filtration chromatography also confirmed the existence of a dimer in solution. The dimeric interface is contributed by helices $\alpha 9$ – $\alpha 11$ and $\alpha 13$ of the lid domain in addition to the loop $_{\alpha 1-\alpha 2}$ [Fig. 1(C)]. In detail, helices $\alpha 9$ – $\alpha 11$ of each subunit form an approximately trilateral interface. Moreover, the loop $_{\alpha 1-\alpha 2}$ of one subunit interacts with the trilateral interface and $\alpha 13$ of the other subunit.

Dali search²³ revealed that BmJHEH mostly resembles mEH members. The top two hits are *Streptomyces carzinostaticus* EH (PDB 4I19, Z-score 2.1, RMSD 0.98 Å over 251 C α atoms) and *A. niger* EH AnEH (PDB 1QO7, Z-score 2.3, RMSD 1.12 Å over 223 C α atoms). Despite sharing similar overall structure and dimerization pattern, BmJHEH and AnEH have two remarkable differences [Fig. 1(D)]. In BmJHEH, the N-terminal membrane-anchor segment (including $\eta 1$) stretches along the protein surface and passes through a shallow groove formed between loop $_{\beta 2-\beta 3}$ and loop $_{\beta 5-\alpha 5}$. By contrast, the N-terminal segment of AnEH without an “XWG” motif is six-residue shorter and adopts a different conformation by extending toward the opposite direction [Fig. 1(D)]. In addition, BmJHEH contains an insertion of helix $\alpha 7$ and $\eta 4$, instead of an eight-residue shorter loop in AnEH. This insertion in BmJHEH, together with helices $\eta 4$, $\alpha 8$, $\alpha 9$, $\alpha 13$, and $\alpha 14$, results in a more stringent substrate-binding pocket [Fig. 1(D)].

The putative substrate-binding pattern

As a typical α/β hydrolase, the active site of BmJHEH also contains a conserved catalytic triad, Asp227, His430, and Glu403. Similar to that of AnEH, the active-site pocket of BmJHEH also contains two tyrosine residues (Tyr298 and Tyr373), which stabilize and donate protons to the oxygen atom of epoxide ring.²⁴ In addition, the H¹⁵²GWP¹⁵⁵ motif in the loop $_{\beta 4-\alpha 4}$ is proposed to facilitate the catalysis by forming a hydrogen bond between the main-chain nitrogen of Trp154 and the nucleophilic residue Asp227.

Beyond the common features of the active site, BmJHEH showed unique structural features to accommodate its favored substrate JHII with a long hydrophobic hydrocarbon chain.²⁵ Electrostatic potential analysis reveals a hydrophobic substrate-binding pocket formed by α -helices ($\alpha 7$ – $\alpha 9$, $\alpha 13$, and $\alpha 14$) from the lid domain, which matches well with its hydrophobic substrate JHII [Fig. 2(A)]. To further elucidate the substrate-binding pattern, we modeled the substrate JHII into the active-site pocket of BmJHEH. In the simulated model [Fig. 2(B)], JHII lies in the hydrophobic pocket with its epoxide ring exposed to the catalytic residue Asp227.

The epoxide ring oxygen (O3) is simultaneously fixed by Tyr298 and Tyr373 via hydrogen bonds, as reported previously.²⁴ The C10 atom has a distance of 2.9 Å from O $\delta 1$ of Asp227, indicating that C10 is ready for the nucleophilic attack by Asp227. This is consistent with the notion that the aspartate residue attacks the epoxide ring carbon of the lowest steric hindrance to form a hydroxyl-alkyl-enzyme intermediate.²⁶ The long hydrophobic hydrocarbon chain of JHII lies along the loop $_{\beta 7-\alpha 7}$, which is rich of hydrophobic residues, such as Met251, Leu253, and Leu255 [Fig. 2(B)]. The variations of the active-site pockets imply that BmJHEH and AnEH catalyze the hydrolysis of different kinds of substrates, further indicating the broad substrate recognition patterns among mEHs.

Multiple-sequence alignment of BmJHEH and homologs revealed that the putative JHII-binding residues are exclusively conserved (Fig. 3). In addition, the N-terminal “XWG” anchor motif, which was proposed as a membrane anchor involved in subcellular localization of BmJHEH in *Bombyx mori*, is highly conserved in higher organisms, but absent from fungi, bacteria, and protozoa (Fig. 3). Moreover, the inserted segments of $\alpha 7$ and $\eta 4$, which play an important role in forming a more stringent substrate-binding pocket, are conserved in mEHs from higher organisms but not in AnEH (Fig. 3). All together, the present structure of BmJHEH provides insights into the substrate recognition and catalysis of mEHs and might be helpful for the design of JH-derived pesticides.

ACKNOWLEDGMENT

We appreciate the help of the staff at the Shanghai Synchrotron Radiation Facility. We are also grateful to all developers of the HADDOCK Program, CCP4i suite, ESPript, and PyMOL.

REFERENCES

1. Roller H, Bjerke JS. Purification and isolation of juvenile hormone and its action in lepidopteran larvae. *Life Sci* 1965;4:1617–1624.
2. Riddiford LM. Cellular and molecular actions of juvenile-hormone .1. General-considerations and premetamorphic actions. *Adv Insect Physiol* 1994;24:213–274.
3. Marchal E, Vandersmissen HP, Badisco L, Van de Velde S, Verlinden H, Iga M, Van Wielendaele P, Huybrechts R, Simonet G, Smagghe G, Vanden Broeck J. Control of ecdysteroidogenesis in prothoracic glands of insects: a review. *Peptides* 2010;31:506–519.
4. Hammock BD. Regulation of juvenile hormone titer. In: Kerkut, GA, Gilbert, LI, editors. *Comprehensive insect physiology, biochemistry and pharmacology*. Oxford: Pergamon Press; 1985. pp 431–472.
5. Share MR, Roe RM. A partition assay for the simultaneous determination of insect juvenile hormone esterase and epoxide hydrolase activity. *Anal Biochem* 1988;169:81–88.
6. Hammock BD, Sparks TC. A rapid assay for insect juvenile hormone esterase activity. *Anal Biochem* 1977;82:573–579.

7. Morisseau C, Hammock BD. Epoxide hydrolases: Mechanisms, inhibitor designs, and biological roles. *Annu Rev Pharmacol Toxicol* 2005;45:311–333.
8. Arand M, Cronin A, Adamska M, Oesch F. Epoxide hydrolases: structure, function, mechanism, and assay. *Methods Enzymol* 2005;400:569–588.
9. Newman JW, Morisseau C, Hammock BD. Epoxide hydrolases: their roles and interactions with lipid metabolism. *Prog Lipid Res* 2005;44:1–51.
10. Zou J, Hallberg BM, Bergfors T, Oesch F, Arand M, Mowbray SL, Jones TA. Structure of *Aspergillus niger* epoxide hydrolase at 1.8 Å resolution: implications for the structure and function of the mammalian microsomal class of epoxide hydrolases. *Structure* 2000;8:111–122.
11. Ollis DL, Cheah E, Cygler M, Dijkstra B, Frolov F, Franken SM, Harel M, Remington SJ, Silman I, Schrag J, Sussman JL, Verschuere KHG, Goldman A. The alpha/beta hydrolase fold. *Protein Eng* 1992;5:197–211.
12. Otwinowski Z, Minor W. Processing of X-ray diffraction data collected in oscillation mode. *Macromol Crystallogr A* 1997;276:307–326.
13. Vagin A, Teplyakov A. Molecular replacement with MOLREP. *Acta Crystallogr D Biol Crystallogr* 2010;66(Pt 1):22–25.
14. Murshudov GN, Vagin AA, Dodson EJ. Refinement of macromolecular structures by the maximum-likelihood method. *Acta Crystallogr D Biol Crystallogr* 1997;53:240–255.
15. Bailey S. The Ccp4 Suite—programs for protein crystallography. *Acta Crystallogr D Biol Crystallogr* 1994;50:760–763.
16. Emsley P, Cowtan K. Coot: model-building tools for molecular graphics. *Acta Crystallogr D Biol Crystallogr* 2004;60(Pt 12 Pt 1):2126–2132.
17. Lovell SC, Davis IW, Arendall WB, 3rd, de Bakker PI, Word JM, Prisant MG, Richardson JS, Richardson DC. Structure validation by Calpha geometry: phi,psi and Cbeta deviation. *Proteins* 2003;50:437–450.
18. DeLano W. The PyMOL molecular graphics system. San Carlos, CA: DeLano Scientific; 2002.
19. de Vries SJ, van Dijk M, Bonvin AM. The HADDOCK web server for data-driven biomolecular docking. *Nat Protoc* 2010;5:883–897.
20. Gilbert LI, Granger NA, Roe RM. The juvenile hormones: historical facts and speculations on future research directions. *Insect Biochem Mol Biol* 2000;30:617–644.
21. Wojtasek H, Prestwich GD. An insect juvenile hormone-specific epoxide hydrolase is related to vertebrate microsomal epoxide hydrolases. *Biochem Biophys Res Commun* 1996;220:323–329.
22. Friedberg T, Lollmann B, Becker R, Holler R, Oesch F. The microsomal epoxide hydrolase has a single membrane signal anchor sequence which is dispensable for the catalytic activity of this protein. *Biochem J* 1994;303(Pt 3):967–972.
23. Holm L, Rosenstrom P. Dali server: Conservation mapping in 3D. *Nucleic acids Res* 2010;38(Web Server issue):W545–W549.
24. Yamada T, Morisseau C, Maxwell JE, Argiriadi MA, Christianson DW, Hammock BD. Biochemical evidence for the involvement of tyrosine in epoxide activation during the catalytic cycle of epoxide hydrolase. *J Biol Chem* 2000;275:23082–23088.
25. Zhang QR, Xu WH, Chen FS, Li S. Molecular and biochemical characterization of juvenile hormone epoxide hydrolase from the silkworm, *Bombyx mori*. *Insect Biochem Mol Biol* 2005;35:153–164.
26. Lacourciere GM, Armstrong RN. The catalytic mechanism of microsomal epoxide hydrolase involves an ester intermediate. *J Am Chem Soc* 1993;115:10466–10467.